

The Resurrection of the ReLU

Coşku Can Horuz^{1*} Geoffrey Kasenbacher^{1,2*} Saya Higuchi¹ Sebastian Kairat¹
 Jendrik Stoltz¹ Moritz Pesl¹ Bernhard A. Moser^{3,4} Christoph Linse⁵
 Thomas Martinetz⁵ Sebastian Otte¹

¹Institute of Robotics and Cognitive Systems, University of Lübeck

²Mercedes-Benz AG

³Software Competence Center Hagenberg (SCCH)

⁴Institute of Signal Processing, Johannes Kepler University of Linz (JKU)

⁵Institute of Neuro- and Bioinformatics, University of Lübeck

{cosku.horuz, sa.higuchi, sebastian.kairat,
 c.linse, thomas.martinetz, sebastian.otte}@uni-luebeck.de
 {jendrik.stoltz, moritz.pesl}@student.uni-luebeck.de
 geoffrey.kasenbacher@mercedes-benz.com
 bernhard.moser@scch.at

Abstract

Modeling sophisticated activation functions within deep learning architectures has evolved into a distinct research direction. Functions such as GELU, SELU, and SiLU offer smooth gradients and improved convergence properties, making them popular choices in state-of-the-art models. Despite this trend, the classical ReLU remains appealing due to its simplicity, inherent sparsity, and other advantageous topological characteristics. However, ReLU units are prone to becoming irreversibly inactive—a phenomenon known as the dying ReLU problem—which limits their overall effectiveness. In this work, we introduce surrogate gradient learning for ReLU (SUGAR) as a novel, plug-and-play regularizer for deep architectures. SUGAR preserves the standard ReLU function during the forward pass but replaces its derivative in the backward pass with a smooth surrogate that avoids zeroing out gradients. We demonstrate that SUGAR, when paired with a well-chosen surrogate function, substantially enhances generalization performance over convolutional network architectures such as VGG-16 and ResNet-18, providing sparser activations while effectively resurrecting dead ReLUs. Moreover, we show that even in modern architectures like Conv2NeXt and Swin Transformer—which typically employ GELU—substituting these with SUGAR yields competitive and even slightly superior performance. These findings challenge the prevailing notion that advanced activation functions are necessary for optimal performance. Instead, they suggest that the conventional ReLU, particularly with appropriate gradient handling, can serve as a strong, versatile revived classic across a broad range of deep learning vision models.

1 Introduction

The choice of activation functions in deep neural networks has a substantial effect on the convergence and performance of a model. Prior to the suggestion to apply Rectified Linear Unit (ReLU) as activation function in [7], concerted effort was made to tackle the saturation and vanishing gradient problem of sigmoidal activations. ReLU has been shown to accelerate convergence and often also

*Equal contribution, corresponding authors.

to enhance generalization. As a landmark moment in deep learning history, ReLU has been used in AlexNet [19], which significantly outperformed its competitors on the ImageNet [3] benchmark. This work explicitly studied the superiority of ReLU over hyperbolic tangent (tanh) in a deep convolution network. Since then, ReLU has been used in numerous tasks including image classification and segmentation, reinforcement learning, natural language processing, and speech recognition [10, 32, 13, 36, 14, 39].

Mathematically, recent research has established a deep connection between tropical geometry and feedforward neural networks with ReLU activations [42], unraveling an underlying algebraic structure of ReLU, namely, tropical semiring that replaces addition with its maximum and multiplication with addition. As a result, the decision boundaries formed by ReLU networks correspond to tropical hypersurfaces, which are the fundamental objects in tropical geometry. Such neural networks are equivalent to tropical rational functions [42], which is defined as a ratio of two tropical polynomials, themselves formed by maxima of affine functions. Closely related to this is the intuitive geometric understanding of consecutive layers of ReLU networks as space folding transformations that allow a compact representation of similarities in the input space [20, 28, 29].

In ReLU networks, the negative pre-activations are silenced with true zeros, which allow sparse representations. This might lead to better generalization on unseen data, but forcing too much sparsity may damage the prediction as it effectively reduces the model capacity [7]. This phenomenon, known as “the dying ReLU problem”, has been a big caveat of ReLU networks. The dying ReLU problem led to a plethora of linear unit functions including, but not limited to LeakyReLU [26], PReLU [9], GELU [11], SELU [17], SiLU/Swish [4, 31], ELU [2]. All these functions introduce non-zero activations for negative pre-activation values, offering different trade-offs between ReLU’s modeling benefits and the advantages of smooth, continuous gradients.

In this paper, we address the limitations of ReLU without sacrificing its advantages by introducing a novel approach: the application of a Surrogate Gradient for ReLU (SUGAR). SUGAR allows models to retain standard ReLU activations, while ensuring stable gradient flow even for negative pre-activations. Further contributions of this work are as follows:

- We propose two new surrogate gradient functions, B-SiLU and NeLU, which integrate seamlessly into a variety of models. These functions consistently improve generalization performance.
- We conduct comprehensive experiments with VGG-16 [35] and ResNet-18 [8], demonstrating that SUGAR significantly enhances generalization in both architectures.
- We evaluate SUGAR on modern architectures such as Swin Transformer [23] and Conv2NeXt [5], showcasing its adaptability and effectiveness.
- An in-depth analysis of VGG-16 layer activations reveals a distinct shift in activation distributions when SUGAR is applied, providing visual evidence for its role in mitigating the dying ReLU problem, while at the same time more sparse representations are fostered.
- We further explore the loss landscape with and without SUGAR, offering deeper insight into its optimization benefits.

The proposed SUGAR method offers several desirable properties. It is simple to implement and consistently utilizes ReLU in the forward pass. When combined with the proposed B-SiLU surrogate function, VGG-16 achieves improvements of 10 and 16 percentage points in test accuracy on CIFAR-10 and CIFAR-100 [18], respectively, while ResNet-18 shows corresponding gains of 9 and 7 percentage points compared to the best-performing models without SUGAR.

2 Background

2.1 Surrogate gradient learning

In conventional artificial neural networks, learning relies on gradient-based optimization methods such as backpropagation, which require continuous, differentiable activation functions. However, spiking neural networks (SNNs) are discrete and non-differentiable, making direct application of backpropagation infeasible.

Surrogate gradient learning emerged as a solution to train SNNs by replacing the gradient of the non-differentiable spiking function with a smooth and differentiable approximation [30]. These surrogate functions allow gradients to flow through the network during training, enabling the use of powerful optimization techniques in neuromorphic and event-based computing settings. This idea gained traction in the late-2010s and has since become a cornerstone for training biologically inspired spiking models in a computationally efficient manner [1, 12, 38, 41].

Recently, a related approach called ProxyGrad [22] improved activation maximization (AM) in convolutional networks by manipulating gradients during optimization. The study showed that using LeakyReLU in the backward pass, while keeping ReLU in the forward pass, enabled AM to escape poor local optima and reach higher activation values. As a result, the method produced more informative and interpretable feature visualizations.

2.2 Forward gradient injection (FGI)

Forward Gradient Injection (FGI) is the backbone algorithm in SUGAR. It was introduced in [34] as a surrogate gradient strategy in SNNs. It exploits the stop gradient operator (i.e. `.detach()`) to manipulate the gradients such that a model with non-differentiable spikes becomes trainable via gradient signals. FGI enables a gradient injection during forward pass with the following equation (indirect surrogate gradient function):

$$y = g(x) - \text{sg}(g(x)) + \text{sg}(f(x)) \quad (1)$$

where $\text{sg}(\cdot)$ is the stop gradient operator, $f(\cdot)$ is the forward computation with its gradient bypassed and $g(\cdot)$ is another function where the gradient is instead injected over the variable of interest x while not contributing to the forward result due subtraction with itself. Choosing $g(\cdot)$ as an activation function with non-zero gradients for negative inputs, ReLU networks can be trained without suffering from the dying ReLU problem. However, Equation 1 requires the gradient computation of $g(\cdot)$ in the backward pass. Following *multiplication trick* allows $\tilde{g}(\cdot)$ to be exactly the derivative of $f(\cdot)$ in the backward pass (direct surrogate gradient function):

$$m = x \cdot \text{sg}(\tilde{g}(x)) \quad (2)$$

$$y = m - \text{sg}(m) + \text{sg}(f(x)) \quad (3)$$

FGI enables the injection of surrogate gradient functions directly in the forward pass, independent of the original function $f(\cdot)$. The results in [34] suggest that FGI can improve both model optimizability and exportability over classical deployments of surrogate gradients (i.e. as overriding the backward function).

3 Surrogate gradient for ReLU (SUGAR)

Our proposed method applies FGI in ReLU networks with smooth surrogate functions. We extend the potential applications of surrogate gradients beyond SNNs, and aim to introduce this framework as a technique to overcome disadvantages of ordinary ReLUs.

Indirect FGI within the context of SUGAR can be expressed as:

$$y = f(x) - \text{sg}(f(x)) + \text{sg}(\text{ReLU}(x)) \quad (4)$$

This formulation enables gradient injection and ensures gradient propagation even for negative activations. Specifically, using the multiplication trick from [34], the direct injection of the surrogate gradient function is accomplished via:

$$m = x \cdot \text{sg}(\tilde{f}(x)) \quad (5)$$

$$y = m - \text{sg}(m) + \text{sg}(\text{ReLU}(x)) \quad (6)$$

Here, $\tilde{f}(x)$ explicitly defines the surrogate gradient behavior for ReLU.

The choice of the surrogate function is flexible and can include activation functions commonly employed in state-of-the-art applications, such as ELU, GELU, SiLU, SELU, and Leaky ReLU (see Figure 8). These functions typically possess desirable properties motivated by mechanisms like self-gating or self-normalization. Importantly, these surrogate candidates share the characteristic of

having non-zero gradients for negative inputs ($x < 0$), unlike ReLU. Although surrogate functions enable gradient flow for negative activations, the forward pass and subsequent loss computation strictly depend on activations for $x > 0$. Consequently, the effect of surrogate gradient learning in this setting can be interpreted as filtering out pre-activations below the cut-off threshold, reducing the network’s propensity to overfit due to topological simplification and sparsity [27, 29], but without harming the gradient flow.

In preliminary studies, we realized the need for adapting the current activation functions to utilize the specific purpose of SUGAR. As it will be discussed in depth later, SUGAR’s effect varies in different regularization settings. Therefore, in the following, we propose two new surrogate functions that align well with these settings.

3.1 B-SiLU

We introduce a novel activation function named Bounded Sigmoid Linear Unit (B-SiLU), which combines self-gating characteristics with a tunable lower bound parameter. Mathematically, this function can be expressed as:

$$\text{B-SiLU}(x) = (x + \alpha) \cdot \sigma(x) - \frac{\alpha}{2}, \quad \text{with } \alpha = 1.67 \quad (7)$$

where $\sigma(x)$ denotes the sigmoid activation. The derivative of the B-SiLU activation function is given by:

$$\frac{d}{dx}\text{B-SiLU}(x) = \sigma(x) + (x + \alpha)\sigma(x)(1 - \sigma(x)) \quad (8)$$

Both B-SiLU and its derivative are visualized in Figure 8. The B-SiLU activation function emerged from exploratory experiments with SUGAR, drawing particular inspiration from the swish-like sigmoidal function introduced in [33] and the related thresholding operator examined in [15, 40]. It is motivated by the goal of combining advantageous properties from the self-gating behavior of SiLU and the smoothness of GELU.

3.2 NeLU

We further introduce Negative slope Linear Unit (NeLU), as a smooth derivative substitute for ReLU. It is inspired by the constant derivative of ReLU for $x > 0$ and a smooth negative slope from GELU for $x < 0$. For large negative inputs, the resulting gradient converges back to zero.

$$\frac{d}{dx}\text{NeLU}(x) = \begin{cases} 1, & \text{if } x > 0 \\ \alpha \frac{2x}{(1 + x^2)^2}, & \text{else} \end{cases} \quad (9)$$

α controls the magnitude of the negative gradient for small values of $x < 0$, which ensures stability. The resulting gradient is shown in Figure 1. By applying the multiplication trick in Equation 5 and Equation 6, it is possible to directly set the gradient of the activation as in Equation 9.

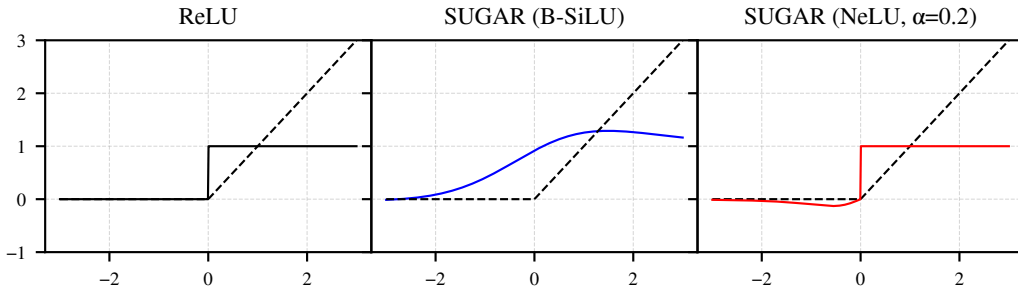


Figure 1: Comparison of activation functions and their derivatives. From left to right: ReLU (dashed) and its derivative (black), ReLU activation function with B-SiLU derivative (blue) and ReLU activation function with NeLU derivative (red).

4 Experiments

4.1 Surrogate function comparison on CIFAR-10/100

We conducted extensive experiments to evaluate and compare various activation functions, both with and without SUGAR, on the CIFAR-10 and CIFAR-100 datasets using ResNet-18 and VGG-16 architectures. In every run where SUGAR is applied, the forward function is always the standard ReLU; for a given surrogate activation f (e.g. ELU), we compare the performance of the network using f in the forward pass and its true gradient in the backward pass (non-SUGAR scenario) against the identical architecture using ReLU for the forward pass but f 's gradient for the backward pass (e.g. SUGAR with ELU). Each configuration was trained five times with different random seeds to ensure robustness of the results. To isolate the generalization effects of the activation functions and the application of SUGAR we did not apply any data augmentation (see Appendix B for the full experimental setup). The set of surrogate functions evaluated included LeakyReLU, SELU, ELU, GELU, SiLU (Swish), Mish, and our proposed B-SiLU and NeLU. See Appendix C for the complete experimental results.

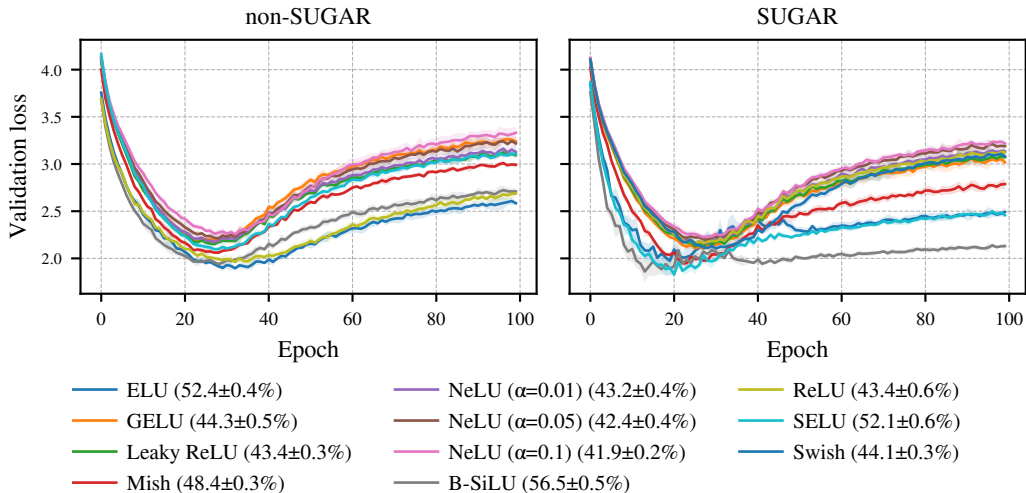


Figure 2: The plots show the validation loss of ResNet-18 on CIFAR-100 with and without SUGAR. In the legend, the corresponding test accuracies (of the respective functions as surrogates) are given for completeness. See Section E.1 for all the convergence plots from the experiments.

Overall, SUGAR with ELU, SELU, and especially B-SiLU delivered the largest gains over the ReLU baseline, whereas LeakyReLU and NeLU consistently underperformed (Figure 2). On CIFAR-10 with a ResNet-18 backbone, B-SiLU rose from 76.76 % to 86.42 % with SUGAR. VGG-16 showed a similar performance: B-SiLU improved the testing accuracy by almost 10 points (78.50 % \rightarrow 88.35 %).

On CIFAR-100, the superiority of SUGAR B-SiLU was even more pronounced: ResNet-18’s accuracy jumped from 48.99 % to 56.51 %, and VGG-16’s from 48.73 % to 64.47 % (Figure 3). Again, Leaky ReLU and NeLU showed negligible or negative gains (e.g. 43.67 % \rightarrow 43.41 % on ResNet-18), indicating that simple linear leakage fails to harness the benefits of SUGAR under this setup. In summary, B-SiLU outperforms all other surrogates across architectures and datasets, ELU and SELU provide reliable improvements, and SUGAR does not benefit meaningfully from Leaky ReLU and NeLU in this setting.

4.2 Stability improvements for deep ReLU networks

To evaluate SUGAR’s effectiveness in addressing the dying ReLU problem, we revisited a controlled setting introduced in [25], where a deep and narrow ReLU network with symmetric weight initialization fails to learn due to widespread neuron inactivity. We replicated and extended the original experiments by incorporating SUGAR with B-SiLU surrogate gradients, which greatly improved

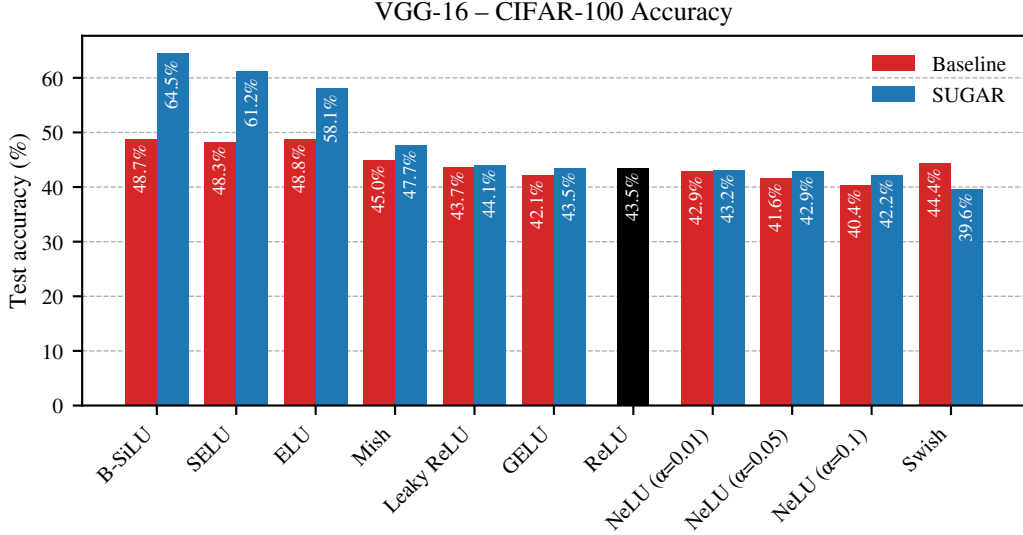


Figure 3: Test accuracy of VGG-16 on CIFAR-100, comparing non-SUGAR (red) and SUGAR (blue) for each activation function. The black bar represents the baseline, where the model is simply trained with ReLU (forward and backward). See Section E.3 for all the accuracy plots from the experiments.

layer activation probabilities and learning outcomes across multiple simple regression tasks. Our results demonstrate that SUGAR enables gradient flow even through inactive neurons, reducing collapse rates and enhancing model expressivity. For an in-depth analysis please refer to Appendix A.

4.3 Conv2NeXt and Swin Transformer

We further investigate SUGAR’s potential in state-of-the-art models. In this regard, we have chosen one convolution and one attention based model. Conv2NeXt [5] was chosen as a convolutional model because it is the same architecture as ConvNeXt [24] but adapted for smaller datasets. Swin Transformer [23] is, on the other hand, a vision transformer model. It is developed for large datasets (i.e. ImageNet1k) and the smallest model has 28M parameters. As we have trained the model on Tiny-ImageNet200 [3], it is considerably over-parameterized for the dataset. The models were adopted in their original form from [23] and [5]. The only modification applied was changing the activation function with the corresponding SUGAR implementation.

When applied to Conv2NeXt, SUGAR consistently outperforms the base models that use GELU in both forward and backward pass, as shown in Table 1. Although our reproduction of the Conv2Next results from [5] stays lower than the reported 83.84% accuracy with GELU, SUGAR with NeLU exceeds this value. In the case of the Swin Transformer, despite a slight drop in performance for B-SiLU, NeLU with $\alpha = 0.01$ yields a higher accuracy than both base models.

Table 1: Top-1 accuracy (%) of Conv2NeXt and Swin Transformer models, trained on CIFAR-100 and Tiny-ImageNet200 respectively. Base models do not apply SUGAR. For both models, the original works apply GELU for the activation. Our proposed equations use ReLU in forward pass. NeLU is reported for different α values. **Best models** are highlighted.

Models	ReLU(base)	GELU(base)	B-SiLU	NeLU(0.01)	NeLU(0.05)	NeLU(0.1)
Conv2NeXt	83.85 \pm 0.2	83.74 \pm 0.2	83.87 \pm 0.2	83.84 \pm 0.1	83.84 \pm 0.3	83.95\pm0.2
Swin Transformer	61.25 \pm 0.1	61.39 \pm 0.5	57.15 \pm 0.2	61.48\pm0.3	61.24 \pm 0.3	61.21 \pm 0.2

5 Discussion

In the subsequent analysis, we examine the SUGAR effect by investigating the layer activations for each sample. The results show a clear shift in the activation distribution. Afterwards, the loss landscape of ResNet-18 is analyzed with and without SUGAR. Finally, we explore the potential of treating SUGAR as a form of regularization.

5.1 SUGAR revives dead neurons

To shed light on how surrogate gradients affect internal representations, we analyzed the activation profiles of a VGG-16 backbone after 40 training epochs on CIFAR-100 (see Figure 4). For each data sample, we recorded how many times a neuron produced an output over the course of an entire training epoch such that the resulting distribution reflects how frequently neurons effectively participate in the forward pass. The frequency at point 0 on the x-axis corresponds to the neurons that are inactive over all samples (i.e. dead neurons).

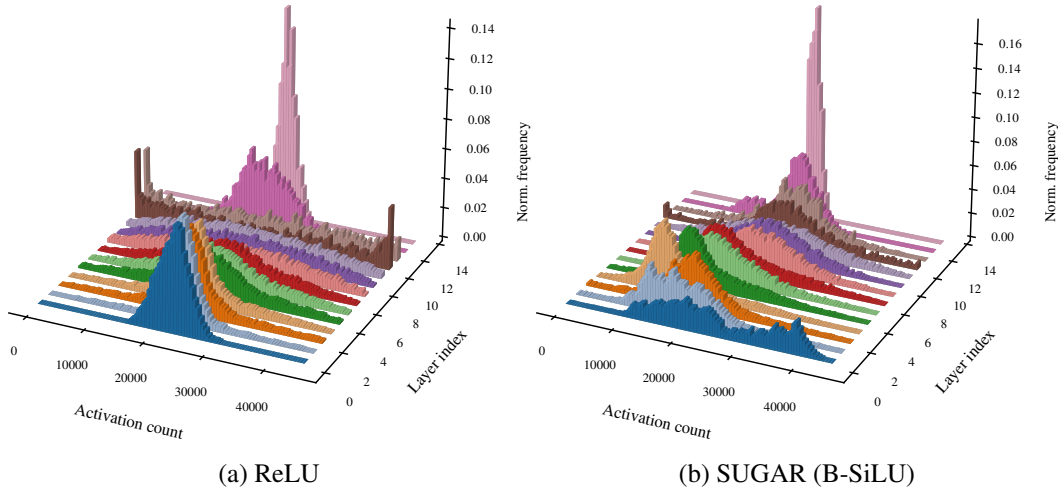


Figure 4: Activation profiles of VGG-16 trained on CIFAR-100 after 40 epochs. The x-axis shows the activation count per data sample, the y-axis indicates the layer index (with the final layer being fully connected), and the z-axis shows the normalized frequency, allowing for comparison across layers and activation functions.

A first striking difference between the vanilla ReLU baseline and the network trained with SUGAR (B-SiLU) appears in layers 12 and 13. The ReLU model shows a flat distribution in the activation-count histogram: a sizable group of neurons never fire (dead neurons) while others remain permanently active. In the SUGAR model, the same layers follow an approximately normal distribution centered on moderate activation counts, indicating that bounded surrogate gradients keep gradient flow alive and prevent neurons from becoming functionally inert.

A second difference concerns the shallow part of the network. The first four convolutional layers of the SUGAR model exhibit slightly flatter, right-skewed distributions whose mode is lower than in the baseline. Hence on average, fewer filters are active for a given image, suggesting that the surrogate-optimized activation encourages selectivity and reduces redundant feature maps, potentially improving generalization.

Taken together, these observations indicate that bounded surrogate gradients simultaneously mitigate the dead-neuron problem and promote sparsity where it is most beneficial. The resulting balance—wide early sparsity combined with well-behaved deep activations—may contribute to the improved generalization reported in Section 4. The reduced average activation rate also hints at tangible gains for deployment on resource-constrained hardware, where memory traffic and multiply-accumulate counts scale with the number of active neurons.

The present analysis is limited to layer-wise aggregate statistics. Future work should track the temporal dynamics of activations during training and evaluate whether the same trends generalize to other architectures and datasets. We observed the same activation-profile patterns on CIFAR-10 across all tested models. The corresponding plots can be found in Section E.2.

5.2 Loss surface analysis

To understand how surrogate gradients reshape the optimization geometry, we visualized the loss landscape in the neighborhood of the trained weights after 10 epochs of training a ResNet-18 on CIFAR-100 (see Figure 5). Following the standard two-direction procedure in [21], we sampled two random directions, rescaled layer-wise to match the ℓ_2 -norm of the corresponding weight tensors (batch-norm parameters frozen). We evaluated the loss on a $100 \times k$ grid spanning $[-0.25, 0.25]^2$ and plotted the resulting contours for the vanilla ReLU model and for the same model trained with SUGAR (B-SiLU).

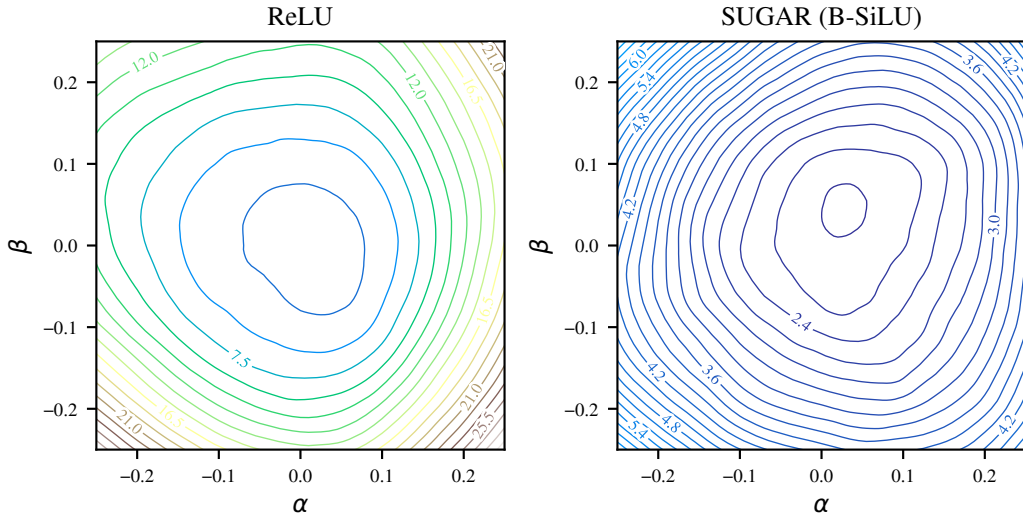


Figure 5: Loss landscapes visualized around the trained solution using different gradient flows. SUGAR (B-SiLU) smooths the optimization surface while retaining the ReLU forward pass, leading to a more stable geometry.

The landscape of the vanilla network exhibits a relatively flat basin at the center but rises steeply toward the edges. At extreme weight perturbations—the corners of the grid—the loss exceeds 25, creating sharp cliffs that can impede optimization. In contrast, the SUGAR landscape is markedly more convex and the loss remains low even at large perturbations. The smoother surface implies better-conditioned gradients and helps explain the faster convergence we observe during training in Figure 2 and Section E.1.

5.3 SUGAR as a regularization technique

The empirical results in Section 5.1 present evidence for a distribution shift in the particular layers. These distributions display sparse activities induced by the ReLU activation function. There is a substantial body of work exploring the relationship between *sparsity* and *generalization* [37, 6]. We aim to examine SUGAR from the perspective of regularization. The most widespread and simple regularization is weight decay, which modulates the gradient of the pure cost function towards small weights. SUGAR also regularizes by modulating the gradient of the pure ReLU-based cost function; however, by employing surrogate activation functions, it does so in a more sophisticated and adaptive manner, depending on the activation patterns.

We consider the investigated models in this work. The results in Section 4.1 and Section 5.1 use models that are not heavily regularized. In this setting, choosing a surrogate function that deviates considerably from ReLU derivative induces harsher regularization and improves the predictive perfor-

mance. However, in a highly regularized setting such as in Section 4.3, additional regularization has to be applied carefully and nuanced to avoid underfitting. In such a scenario, it is advisable to choose a function (e.g. NeLU) that deviates only slightly from the ReLU’s derivative providing gradient flow for pre-activation below the cut-off threshold while modeling the backward characteristics of ReLU as closely as possible. This behavior is reflected in our results: while B-SiLU leads to substantial improvements in generalization for VGG-16 and ResNet-18 (see Section 4.1), NeLU proves to be more effective in enhancing generalization in the already regularized Conv2NeXt and Swin Transformer models (see Section 4.3).

6 Conclusion

This work provides compelling evidence that surrogate gradient learning, originally applied in the spiking neural network domain, can significantly benefit the classical ReLUs in non-spiking deep neural networks. By preserving ReLU in the forward pass while substituting its derivative with a smooth surrogate function during backpropagation, SUGAR enables robust training dynamics and improved generalization, especially in convolutional architectures like VGG-16 and ResNet-18.

Our findings suggest that SUGAR, combined with carefully designed surrogate functions such as B-SiLU and NeLU, offers an elegant solution to the long-standing dying ReLU problem. B-SiLU, in particular, introduces bounded smooth gradients that not only prevent neuron inactivity but also encourage beneficial sparsity patterns. NeLU, on the other hand, offers a more conservative regularization effect through its smooth negative slope, preserving ReLU’s structural simplicity and beneficial properties while improving gradient flow for suppressed activations.

Although the exact influence of NeLU’s negative slope on training dynamics remains an open question, our experiments indicate that it contributes to gradient propagation in strongly regularized models like Conv2NeXt and Swin Transformer. This suggests a nuanced interaction between surrogate gradient shape and model regularization strength, pointing to promising avenues for future exploration.

In conclusion, this work repositions classical ReLU not as a relic, but as a resilient component in the deep learning toolbox. With appropriate gradient handling, ReLU-based networks can match or even outperform modern architectures that rely on more complex activations.

6.1 Limitations and future work

SUGAR’s performance varies notably across different model families. It shows clear benefits in deep, less-regularized networks like VGG-16 and ResNet-18 but is less effective, or even detrimental, in highly regularized architectures such as Conv2NeXt and Swin Transformer, if the surrogate gradient strongly deviates from the ReLU derivative.

The surrogate functions introduced were crafted through empirical intuition and trial-based tuning rather than grounded in formal design principles. Moreover, our results suggest improvements in training dynamics and generalization, but the study does not yet offer formal guarantees on convergence, stability, or generalization bounds. Without a rigorous analytical framework, it is difficult to predict SUGAR’s behavior across different training regimes.

Our evaluation focuses primarily on image classification tasks using datasets like CIFAR-10, CIFAR-100, and Tiny-ImageNet, in addition to few toy problems. It is uncertain how SUGAR would perform in other domains such as natural language processing, reinforcement learning, or time series modeling, where activation dynamics and gradient propagation can differ substantially.

Beyond addressing the current limitations and open questions, future research may assess automatic surrogate function search tailored for specific architectures and datasets. It may also be interesting to consider dynamic surrogates that adapt based on training signals and activation distributions, or in a scheduled manner.

Moreover, given that SUGAR improves sparsity and reduces the activation profiles within the network while applying just simple ReLU, it may prove beneficial for structured pruning, quantization-aware training, or energy-efficient inference in the context of low-footprint models.

References

- [1] Guillaume Bellec, Darjan Salaj, Anand Subramoney, Robert Legenstein, and Wolfgang Maass. Long short-term memory and learning-to-learn in networks of spiking neurons. *Advances in neural information processing systems*, 31, 2018.
- [2] Djork-Arné Clevert, Thomas Unterthiner, and Sepp Hochreiter. Fast and accurate deep network learning by exponential linear units (elus). In *International Conference on Learning Representations (ICLR)*, 2016.
- [3] Jia Deng, Wei Dong, Richard Socher, Li-Jia Li, Kai Li, and Li Fei-Fei. Imagenet: A large-scale hierarchical image database. In *2009 IEEE conference on computer vision and pattern recognition*, pages 248–255. Ieee, 2009.
- [4] Stefan Elfving, Eiji Uchibe, and Kenji Doya. Sigmoid-weighted linear units for neural network function approximation in reinforcement learning. *Neural Networks*, 107:3–11, 2018. Special issue on deep reinforcement learning.
- [5] Jianwei Feng, Hengliang Tan, Wangwang Li, and Ming Xie. Conv2next: Reconsidering conv next network design for image recognition. In *2022 International Conference on Computers and Artificial Intelligence Technologies (CAIT)*, pages 53–60, 2022.
- [6] Trevor Gale, Erich Elsen, and Sara Hooker. The state of sparsity in deep neural networks. *arXiv preprint arXiv:1902.09574*, 2019.
- [7] Xavier Glorot, Antoine Bordes, and Yoshua Bengio. Deep sparse rectifier neural networks. In Geoffrey Gordon, David Dunson, and Miroslav Dudík, editors, *Proceedings of the Fourteenth International Conference on Artificial Intelligence and Statistics*, volume 15 of *Proceedings of Machine Learning Research*, pages 315–323, Fort Lauderdale, FL, USA, 11–13 Apr 2011. PMLR.
- [8] Kaiming He, X. Zhang, Shaoqing Ren, and Jian Sun. Deep residual learning for image recognition. *2016 IEEE Conference on Computer Vision and Pattern Recognition (CVPR)*, pages 770–778, 2015.
- [9] Kaiming He, Xiangyu Zhang, Shaoqing Ren, and Jian Sun. Delving deep into rectifiers: Surpassing human-level performance on imagenet classification. In *2015 IEEE International Conference on Computer Vision (ICCV)*, pages 1026–1034, 2015.
- [10] Kaiming He, Xiangyu Zhang, Shaoqing Ren, and Jian Sun. Deep residual learning for image recognition. In *Proceedings of the IEEE conference on computer vision and pattern recognition*, pages 770–778, 2016.
- [11] Dan Hendrycks and Kevin Gimpel. Gaussian error linear units (gelus). *arXiv preprint arXiv:1606.08415*, 2016.
- [12] Saya Higuchi, Sebastian Kairat, Sander Bohté, and Sebastian Otte. Balanced resonate-and-fire neurons. In *Proceedings of the 41st International Conference on Machine Learning*, volume 235 of *Proceedings of Machine Learning Research*, pages 18305–18323. PMLR, 21–27 Jul 2024.
- [13] Andrew Jesson, Chris Lu, Gunshi Gupta, Nicolas Beltran-Velez, Angelos Filos, Jakob N. Foerster, and Yarin Gal. Relu to the rescue: improve your on-policy actor-critic with positive advantages. In *Proceedings of the 41st International Conference on Machine Learning, ICML’24*. JMLR.org, 2024.
- [14] Nandan Kumar Jha and Brandon Reagan. Relu’s revival: On the entropic overload in normalization-free large language models. *2nd Workshop on Attributing Model Behavior at Scale (NeurIPS)*, 2024.
- [15] Geoffrey Kasenbacher, Felix Ehret, Gerrit Ecke, and Sebastian Otte. Warp-lca: Efficient convolutional sparse coding with locally competitive algorithm. *Neurocomputing*, page 130291, 2025.
- [16] Diederik P Kingma and Jimmy Ba. Adam: A method for stochastic optimization. *arXiv preprint arXiv:1412.6980*, 2014.
- [17] Günter Klambauer, Thomas Unterthiner, Andreas Mayr, and Sepp Hochreiter. Self-normalizing neural networks. In *Advances in neural information processing systems (NIPS)*, volume 30, 2017.
- [18] Alex Krizhevsky. Learning multiple layers of features from tiny images. Master’s thesis, Department of Computer Science, University of Toronto, 2009.
- [19] Alex Krizhevsky, Ilya Sutskever, and Geoffrey E Hinton. Imagenet classification with deep convolutional neural networks. In F. Pereira, C.J. Burges, L. Bottou, and K.Q. Weinberger, editors, *Advances in Neural Information Processing Systems*, volume 25. Curran Associates, Inc., 2012.

- [20] Michal Lewandowski, Hamid Eghbalzadeh, Bernhard Heinzl, Raphael Pisoni, and Bernhard A. Moser. On space folds of reLU neural networks. *Transactions on Machine Learning Research*, 2025.
- [21] Hao Li, Zheng Xu, Gavin Taylor, Christoph Studer, and Tom Goldstein. Visualizing the loss landscape of neural nets. *Advances in neural information processing systems*, 31, 2018.
- [22] Christoph Linse, Erhardt Barth, and Thomas Martinetz. Leaky relus that differ in forward and backward pass facilitate activation maximization in deep neural networks. In *2024 International Joint Conference on Neural Networks (IJCNN)*, pages 1–8, 2024.
- [23] Ze Liu, Yutong Lin, Yue Cao, Han Hu, Yixuan Wei, Zheng Zhang, Stephen Lin, and Baining Guo. Swin transformer: Hierarchical vision transformer using shifted windows. *2021 IEEE/CVF International Conference on Computer Vision (ICCV)*, pages 9992–10002, 2021.
- [24] Zhuang Liu, Hanzi Mao, Chao-Yuan Wu, Christoph Feichtenhofer, Trevor Darrell, and Saining Xie. A convnet for the 2020s. In *2022 IEEE/CVF Conference on Computer Vision and Pattern Recognition (CVPR)*, pages 11966–11976, 2022.
- [25] Lu Lu, Yeonjong Shin, Yanhui Su, and George Em Karniadakis. Dying relu and initialization: Theory and numerical examples. *Communications in Computational Physics*, 28(5):1671–1706, January 2020.
- [26] Andrew L Maas, Awni Y Hannun, and Andrew Y Ng. Rectifier nonlinearities improve neural network acoustic models. In *Proc. ICML workshop track*, volume 30, 2013.
- [27] Dushyant Mehta, Kwang In Kim, and Christian Theobalt. On implicit filter level sparsity in convolutional neural networks. In *Proceedings of the IEEE/CVF Conference on Computer Vision and Pattern Recognition (CVPR)*, pages 520–528, 2019.
- [28] Guido Montúfar, Razvan Pascanu, Kyunghyun Cho, and Yoshua Bengio. On the number of linear regions of deep neural networks. In *Proceedings of the 28th International Conference on Neural Information Processing Systems - Volume 2, NIPS’14*, page 2924–2932, Cambridge, MA, USA, 2014. MIT Press.
- [29] Gregory Naitzat, Andrey Zhitnikov, and Lek-Heng Lim. Topology of deep neural networks. *J. Mach. Learn. Res.*, 21(1), January 2020.
- [30] Emre O. Neftci, Hesham Mostafa, and Friedemann Zenke. Surrogate gradient learning in spiking neural networks: Bringing the power of gradient-based optimization to spiking neural networks. *IEEE Signal Processing Magazine*, 36:51–63, 2019.
- [31] Prajit Ramachandran, Barret Zoph, and Quoc V Le. Searching for activation functions. In *6th International Conference on Learning Representations, ICLR 2018, Workshop Track Proceedings*, 2018.
- [32] Olaf Ronneberger, Philipp Fischer, and Thomas Brox. U-net: Convolutional networks for biomedical image segmentation, 2015.
- [33] Christopher J Rozell, Don H Johnson, Richard G Baraniuk, and Bruno A Olshausen. Sparse coding via thresholding and local competition in neural circuits. *Neural computation*, 20(10):2526–2563, 2008.
- [34] Otte Sebastian. Flexible and efficient surrogate gradient modeling with forward gradient injection. In *The First Austrian Symposium on AI, Robotics, and Vision 2024 (AIROV24)*, pages 451–459, 2024.
- [35] Karen Simonyan and Andrew Zisserman. Very deep convolutional networks for large-scale image recognition. *arXiv preprint arXiv:1409.1556*, 2014.
- [36] Ashish Vaswani, Noam Shazeer, Niki Parmar, Jakob Uszkoreit, Llion Jones, Aidan N Gomez, Łukasz Kaiser, and Illia Polosukhin. Attention is all you need. *Advances in neural information processing systems*, 30, 2017.
- [37] Wei Wen, Chunpeng Wu, Yandan Wang, Yiran Chen, and Hai Li. Learning structured sparsity in deep neural networks. *Advances in neural information processing systems*, 29, 2016.
- [38] Bojian Yin, Federico Corradi, and Sander M Bohté. Accurate and efficient time-domain classification with adaptive spiking recurrent neural networks. *Nature Machine Intelligence*, 3(10):905–913, 2021.
- [39] M.D. Zeiler, M. Ranzato, R. Monga, M. Mao, K. Yang, Q.V. Le, P. Nguyen, A. Senior, V. Vanhoucke, J. Dean, and G.E. Hinton. On rectified linear units for speech processing. In *2013 IEEE International Conference on Acoustics, Speech and Signal Processing*, pages 3517–3521, 2013.
- [40] Jinshan Zeng, Shaobo Lin, Yao Wang, and Zongben Xu. $l_{\{1/2\}}$ regularization: Convergence of iterative half thresholding algorithm. *IEEE Transactions on Signal Processing*, 62(9):2317–2329, 2014.

- [41] Friedemann Zenke and Tim P Vogels. The remarkable robustness of surrogate gradient learning for instilling complex function in spiking neural networks. *Neural computation*, 33(4):899–925, 2021.
- [42] Liwen Zhang, Gregory Naitzat, and Lek-Heng Lim. Tropical geometry of deep neural networks. In Jennifer G. Dy and Andreas Krause, editors, *Proceedings of the 35th International Conference on Machine Learning, ICML 2018, Stockholmsmässan, Stockholm, Sweden, July 10-15, 2018*, volume 80 of *Proceedings of Machine Learning Research*, pages 5819–5827. PMLR, 2018.

A A toy example for solving the dying ReLU problem with SUGAR

In [25], a deliberate setting for dying ReLUs was created. Under the given configuration, a 10-layered ReLU network produced constant output due to the dying ReLU problem. The proposed solution is Randomized Asymmetric Initialization (RAI) of the weights such that there are fewer negative activations. In this section, we replicate and augment these experiments with SUGAR and show that SUGAR is able to dramatically reduce the probability of dead activations.

The network in question consists of 10 feedforward hidden layers with a width of 2, which only employs ReLU activations. As shown in [25], when a neural network is sufficiently deep relative to its width and initialized with symmetric weights, the initial activation probabilities tend to be near zero. In that case, in more than 90% of trials, the network fails to learn meaningful representations due to widespread irrevocable neuron inactivity.

To conduct the evaluation, four distinct toy datasets in the range of $[-1.5, 1.5]$ were adapted from [25] as regression tasks. For each function, we drew 3000 samples from $\mathcal{U}[-\sqrt{3}, \sqrt{3}]^{d_{in}}$, used as input for the network. d_{in} denotes the input dimension which is 2 for Equation 13 and 1 for the rest. For each task, 100 independent runs were carried out. The corresponding equations are as follows:

$$f_1(x) = |x| \quad (10)$$

$$f_2(x) = x \cdot \sin(5x) \quad (11)$$

$$f_3(x) = \mathbb{1}_{\{x>0\}}(x) + 0.2 \sin(5x) \quad (12)$$

$$f_4(x_1, x_2) = \begin{bmatrix} x_1 + x_2 \\ x_1 - x_2 \end{bmatrix} \quad (13)$$

The loss was calculated as the mean squared error over 250 epochs. Adam [16] was used as an optimizer with a learning rate of 0.005 and being decreased by 0.1 in epochs 100, 150, 200, 225. The minibatch size is 64 for every target function. As surrogate gradient in this experiment, the derivation of B-SiLU is used.

Figure 6 illustrates clearly that the ReLU network fails to solve the regression task on Equation 10 as has already been shown in [25]. Once SUGAR with B-SiLU is applied, the network produces much more activation and is able to solve the regression task.

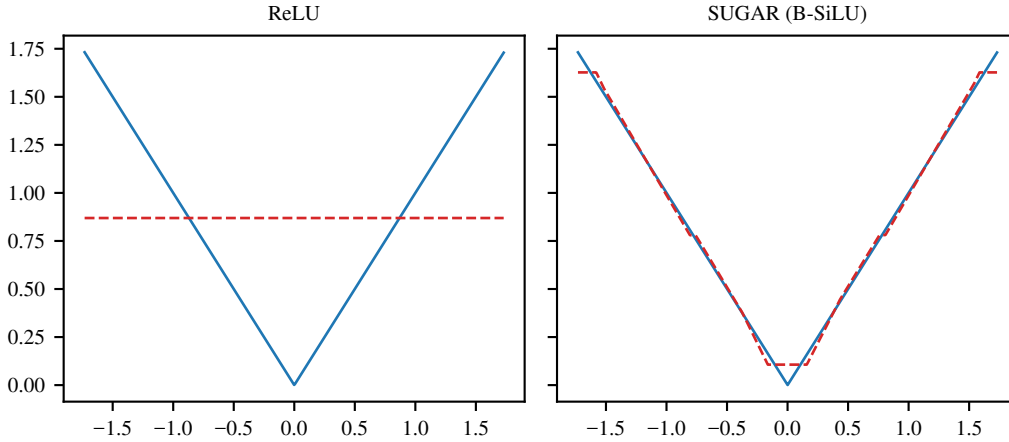


Figure 6: Exemplary comparison of predictions. Left plot shows the prediction of the plain ReLU network whereas SUGAR with B-SiLU is applied on the right.

In addition, we tracked the mean layer activation probabilities, as shown in Figure 7, in order to monitor activity within each layer and estimate the number of neurons actively contributing during the forward pass. As a result, we obtained a dynamic view of the network’s internal activity, allowing us to assess whether the network utilized its capacity effectively and how sparsity evolved during

learning. A model with low activation in early layers might struggle to propagate information, while excessively high activation in later layers may indicate redundancy. Nonetheless, for the sake of clarity, we only visualize the average activities across all layers.

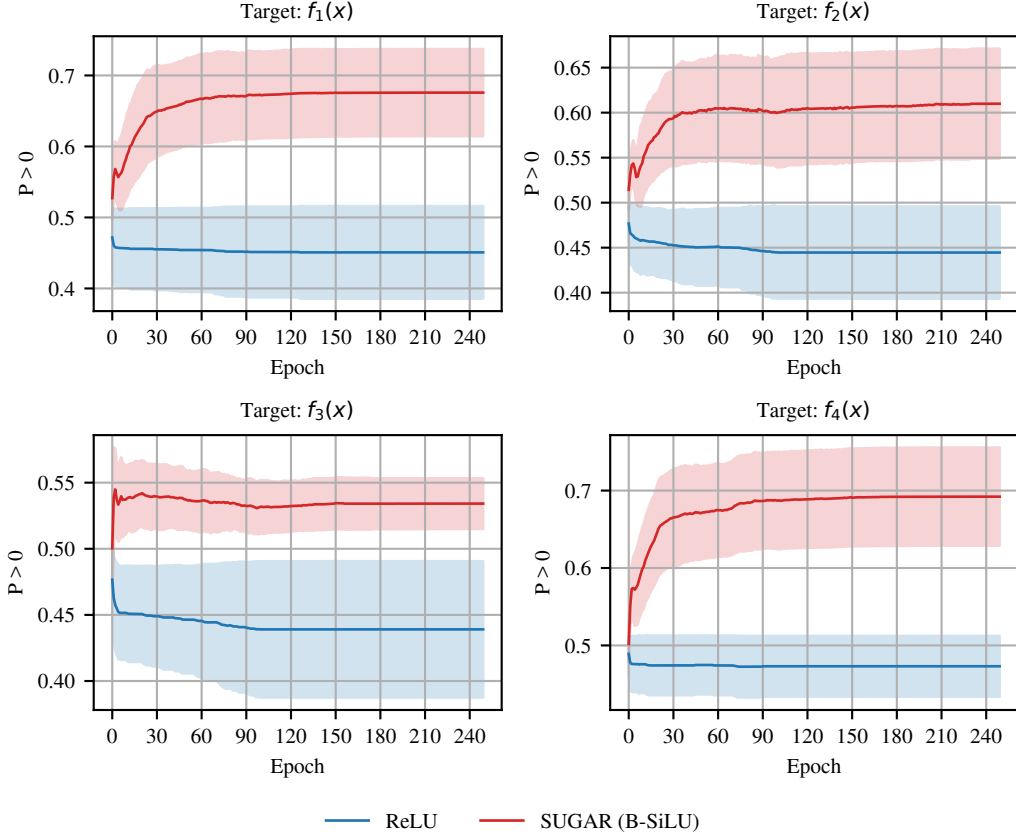


Figure 7: Layer activation probabilities averaged over all runs and layers for each method and task. The plots indicate that SUGAR with B-SiLU increase the activations over all layers during training while the use of standard ReLU only leads to a loss or stagnation of layer activity.

In [25], the number of layers for Equation 13 is increased to 20 from 10 due to the complexity of the equation. In SUGAR experiments, the layer number is kept at 10 and the model still generated more activation across layers compared to the results given in [25], as shown in Table 2. Using asymmetric positive initialization method, as suggested in [25], reduces the possibility of the neurons becoming inactive. However, once a neuron is inactive, there is no possibility for the model to reactivate the neuron due to the fact that the proposed method only concerns the initialization. For SUGAR, it is still possible as a results of the enabled gradient flow through that particular neuron.

Table 2: Empirical probabilities in % from 100 independent simulations of the network to collapse and learn nothing (A), to learn features to some degree (B) and to successfully approximate the target function (C) as indicated in [25]. Results annotated with * are taken from [25] which conducted 1.000 independent simulations. For the last three target functions, [25] categorized the results only into (A) and not collapsed (D) which is also adapted here. **Best models** are highlighted. The respective loss ranges are decomposed in Table 3.

Target function f_i	Method	(A)	(B)	(C)	(D)
$f_1(x)$	Symmetric (He init)*	93.6	4.2	2.2	-
	RAI*	40.3	22.4	37.3	-
	B-SiLU	15.0	8.0	77.0	-
$f_2(x)$	Symmetric (He init)*	91.9	-	-	8.1
	RAI*	29.2	-	-	70.8
	B-SiLU	9.0	-	-	91.0
$f_3(x)$	Symmetric (He init)*	93.8	-	-	6.2
	RAI*	32.6	-	-	67.4
	B-SiLU	2.0	-	-	98.0
$f_4(x_1, x_2)$	Symmetric (He init)*	76.8	-	-	23.2
	RAI*	9.6	-	-	90.4
	B-SiLU	8.0	-	-	92.0

Table 3: Each run was assigned to a category by dividing the resulting loss histogram into the respective number of sections. This table provides the loss ranges which were assigned to each category. Note that no loss was observed outside the reported ranges.

Target function f_i	Category	Loss range
$f_1(x)$	(A)	$15.5818 \leq \mathcal{L} \leq 15.7392$
	(B)	$10.5453 \leq \mathcal{L} \leq 11.0175$
	(C)	$0.0003 \leq \mathcal{L} \leq 0.6299$
	(D)	-
$f_2(x)$	(A)	$36.2548 \leq \mathcal{L} \leq 36.6155$
	(B)	-
	(C)	-
	(D)	$0.5452 \leq \mathcal{L} \leq 27.2373$
$f_3(x)$	(A)	$19.2409 \leq \mathcal{L} \leq 19.4284$
	(B)	-
	(C)	-
	(D)	$0.6767 \leq \mathcal{L} \leq 1.4268$
$f_4(x)$	(A)	$81.0379 \leq \mathcal{L} \leq 81.5630$
	(B)	-
	(C)	-
	(D)	$29.0563 \leq \mathcal{L} \leq 64.7609$

B Experimental setup for VGG-16 and ResNet-18

All activation-function experiments on CIFAR-10 and CIFAR-100 were run with identical settings:

- **Batch size:** 128
- **Validation split:** 10% of the training set
- **Data augmentation:** None
- **Number of workers:** 4
- **Optimizer:** SGD with learning rate 0.001
- **LR schedule:** single milestone at epoch 100
- **Epochs:** 50 for CIFAR-10, 100 for CIFAR-100
- **Repetitions:** 5 independent runs per configuration with seeds [1, 10, 20, 25, 42]
- **Hardware:** NVIDIA RTX A6000 GPUs (CUDA 12.6, Driver 560.35.03)

C Complete results for VGG-16 and ResNet-18 on CIFAR-10/100

In this section the full results of VGG-16 and ResNet-18 are provided. Strikingly, when ReLU and B-SiLU join forces, they excel at generalization.

Table 4: Test accuracy statistics for ResNet-18 and VGG-16 on CIFAR-10. **Best model** and the **second best model** are highlighted.

Model	Activation	non-SUGAR (%)	SUGAR (%)
ResNet-18	ELU	77.91 ± 0.49	83.47 ± 0.62
	GELU	71.57 ± 0.52	73.89 ± 0.39
	LeakyReLU	73.08 ± 0.33	73.84 ± 0.16
	Mish	74.24 ± 0.22	79.19 ± 0.25
	B-SiLU	76.76 ± 0.52	86.42 ± 0.33
	ReLU	73.22 ± 0.42	—
	SELU	75.90 ± 0.63	81.95 ± 0.21
	NeLU($\alpha = 0.01$)	73.01 ± 0.32	73.08 ± 0.42
	NeLU($\alpha = 0.05$)	71.01 ± 0.55	72.12 ± 0.41
	NeLU($\alpha = 0.1$)	69.42 ± 0.34	71.09 ± 0.59
	Swish	73.91 ± 0.49	73.85 ± 0.22
VGG-16	ELU	78.87 ± 0.43	85.58 ± 0.16
	GELU	75.03 ± 0.45	75.86 ± 0.25
	LeakyReLU	75.74 ± 0.71	76.04 ± 0.26
	Mish	76.43 ± 0.30	78.98 ± 0.33
	B-SiLU	78.50 ± 0.25	88.35 ± 0.26
	ReLU	75.85 ± 0.51	—
	SELU	78.28 ± 0.34	86.87 ± 0.28
	NeLU($\alpha = 0.01$)	75.54 ± 0.30	75.88 ± 0.23
	NeLU($\alpha = 0.05$)	74.61 ± 0.19	75.50 ± 0.33
	NeLU($\alpha = 0.1$)	73.19 ± 0.53	74.75 ± 0.17
	Swish	75.92 ± 0.48	72.81 ± 0.48

Table 5: Test accuracy statistics for ResNet-18 and VGG-16 on CIFAR-100. **Best model** and the **second best model** are made salient with the corresponding colors.

Model	Activation	non-SUGAR (%)	SUGAR (%)
ResNet-18	ELU	49.91 \pm 0.56	52.38 \pm 0.37
	GELU	41.55 \pm 0.43	44.30 \pm 0.51
	LeakyReLU	43.67 \pm 0.44	43.41 \pm 0.28
	Mish	44.61 \pm 0.32	48.37 \pm 0.30
	B-SiLU	48.99 \pm 0.78	56.51 \pm 0.46
	ReLU	43.38 \pm 0.57	—
	SELU	48.73 \pm 0.80	52.08 \pm 0.58
	NeLU($\alpha = 0.01$)	42.82 \pm 0.82	43.21 \pm 0.38
	NeLU($\alpha = 0.05$)	41.52 \pm 0.67	42.40 \pm 0.42
	NeLU($\alpha = 0.1$)	40.42 \pm 0.39	41.94 \pm 0.17
	Swish	43.71 \pm 0.43	44.05 \pm 0.26
VGG-16	ELU	48.76 \pm 0.40	58.09 \pm 0.40
	GELU	42.12 \pm 0.11	43.51 \pm 0.55
	LeakyReLU	43.68 \pm 0.42	44.11 \pm 0.30
	Mish	44.96 \pm 0.37	47.74 \pm 0.12
	B-SiLU	48.73 \pm 0.21	64.47 \pm 0.32
	ReLU	43.48 \pm 0.36	—
	SELU	48.34 \pm 0.11	61.20 \pm 0.50
	NeLU($\alpha = 0.01$)	42.89 \pm 0.21	43.18 \pm 0.28
	NeLU($\alpha = 0.05$)	41.58 \pm 0.29	42.85 \pm 0.20
	NeLU($\alpha = 0.1$)	40.35 \pm 0.88	42.19 \pm 0.47
	Swish	44.39 \pm 0.44	39.59 \pm 0.31

D Activation functions and their derivatives

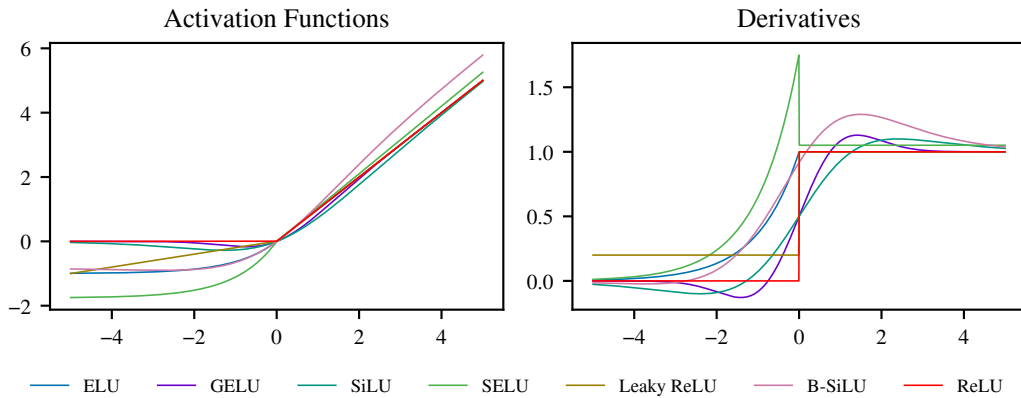


Figure 8: Comparison of activation functions and their derivatives used in modern neural networks. The left plot shows the functional forms of ELU, GELU, SiLU, SELU, Leaky ReLU (with slope 0.2), B-SiLU, and ReLU. The right plot shows their respective derivatives. ReLU and B-SiLU are overlaid for visual prominence. Notably, non-linear smooth activations exhibit continuous derivatives, while ReLU and its variants introduce discontinuities or sharp transitions. Axis labels denote input x and activation output $f(x)$ or its derivative $f'(x)$.

E Additional plots from VGG-16 and ResNet-18 experiments

This appendix presents additional plots to provide deeper insight into the convergence behavior, activation profile, and test accuracy observed in the experiments with VGG-16 and ResNet-18.

E.1 Validation curve plots

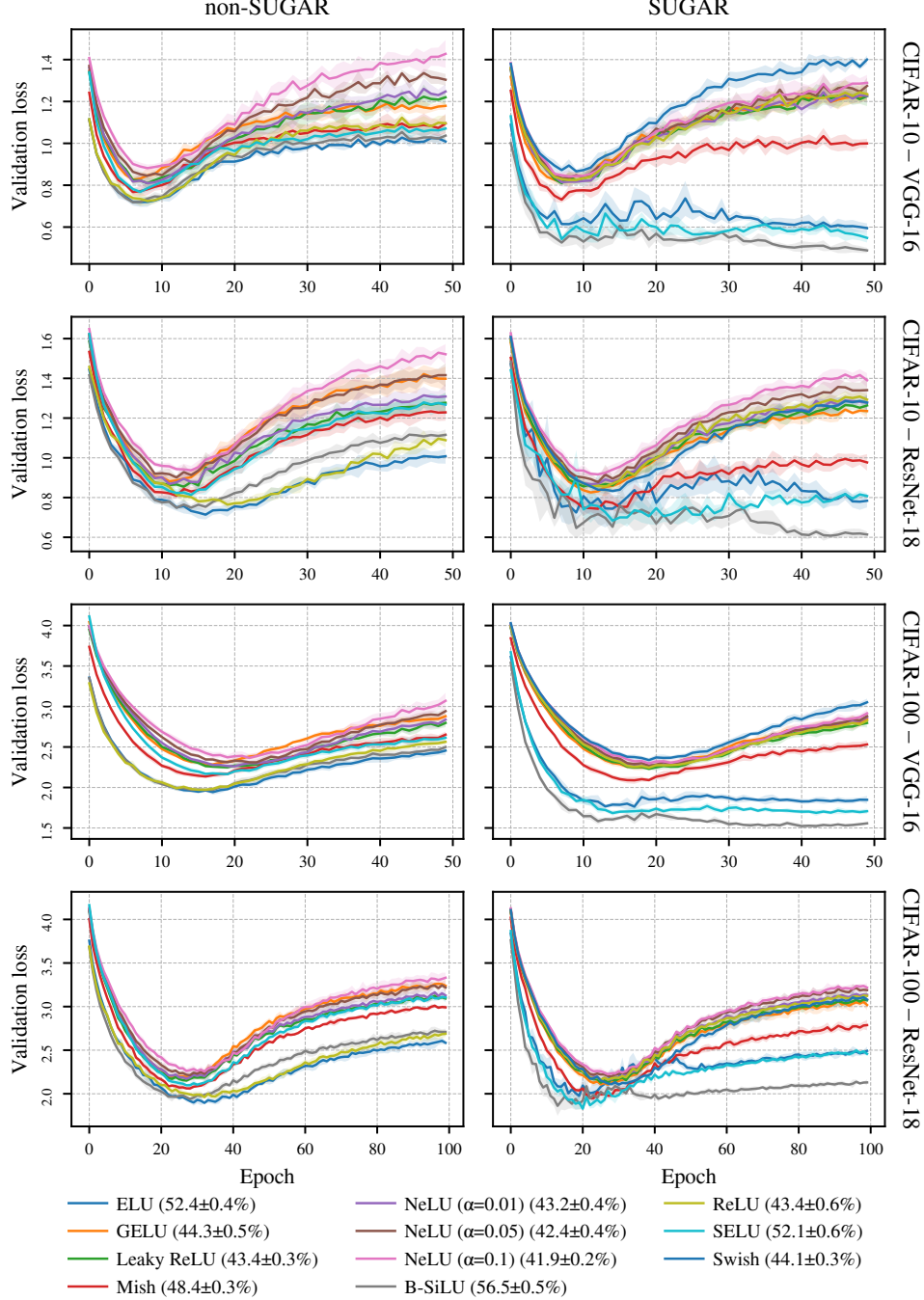
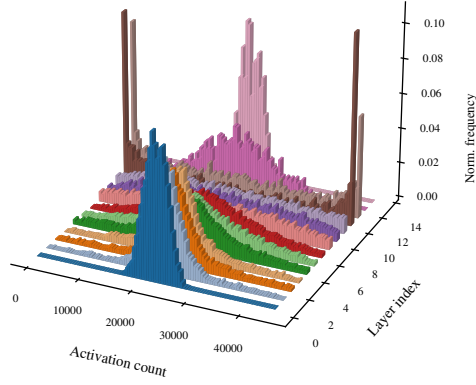
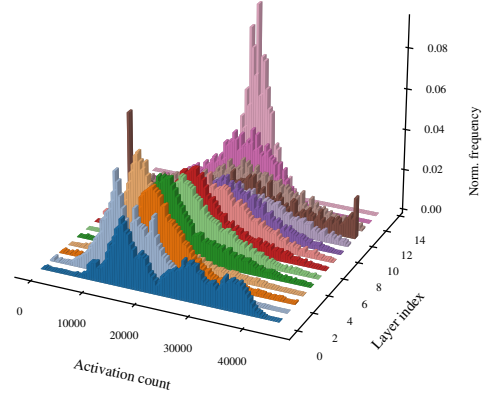


Figure 9: Mean validation-loss curves for CIFAR-10/100 on VGG-16 and ResNet-18 with confidence intervals. Each experiment pair (row) shares its own log-scaled y -axis; experiment titles are displayed vertically on the right-hand plot in each row.

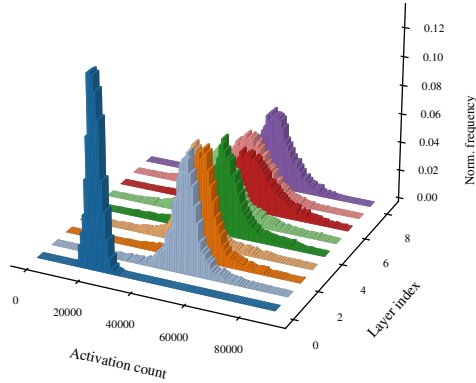
E.2 Activation plots



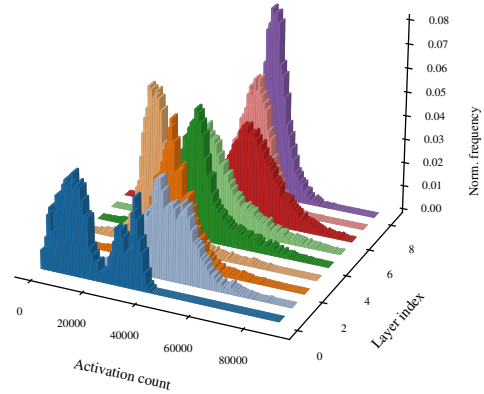
(a) ReLU (CIFAR-10, VGG-16)



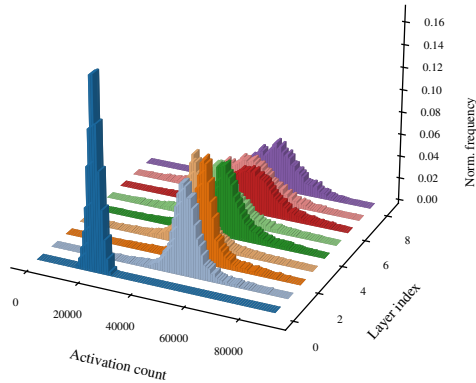
(b) SUGAR B-SiLU (CIFAR-10, VGG-16)



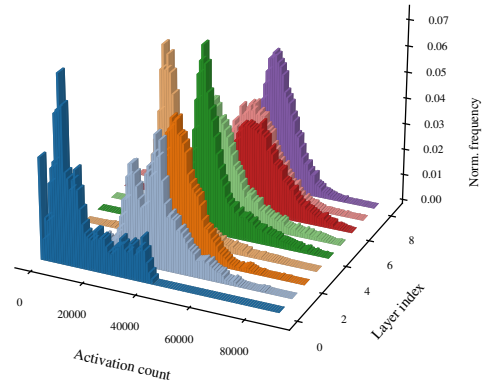
(c) ReLU (CIFAR-100, ResNet-18)



(d) SUGAR B-SiLU (CIFAR-100, ResNet-18)



(e) ReLU (CIFAR-10, ResNet-18)



(f) SUGAR B-SiLU (CIFAR-10, ResNet-18)

Figure 10: Activation profiles of ReLU and SUGAR B-SiLU for VGG-16 and ResNet-18 trained on CIFAR-10 and CIFAR-100. The x-axis shows the activation count per data sample, the y-axis indicates the layer index (with the final layer being fully connected), and the z-axis shows the normalized frequency, allowing for comparison across layers and activation functions.

E.3 Bar chart accuracies

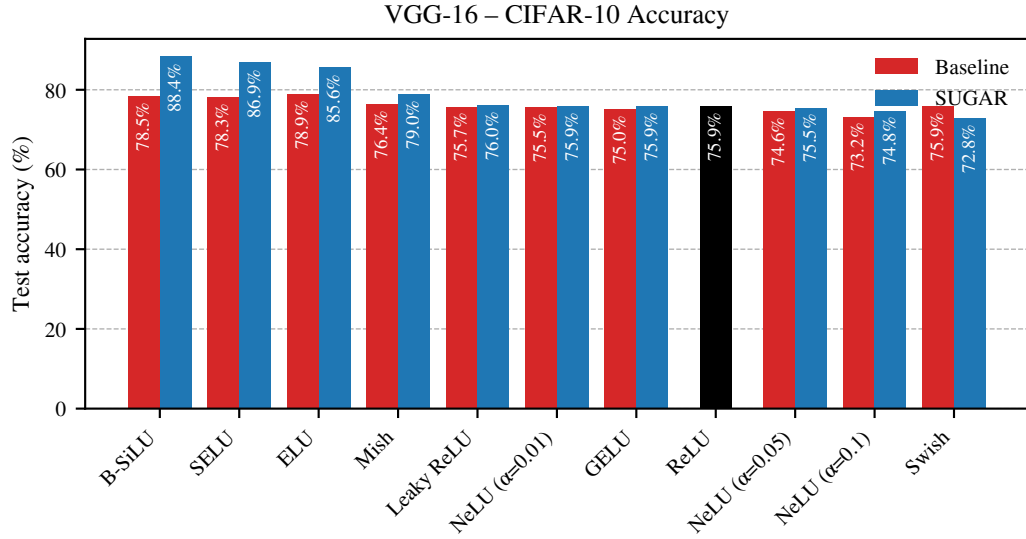


Figure 11: Test accuracy of VGG-16 on CIFAR-10, comparing baseline to SUGAR.

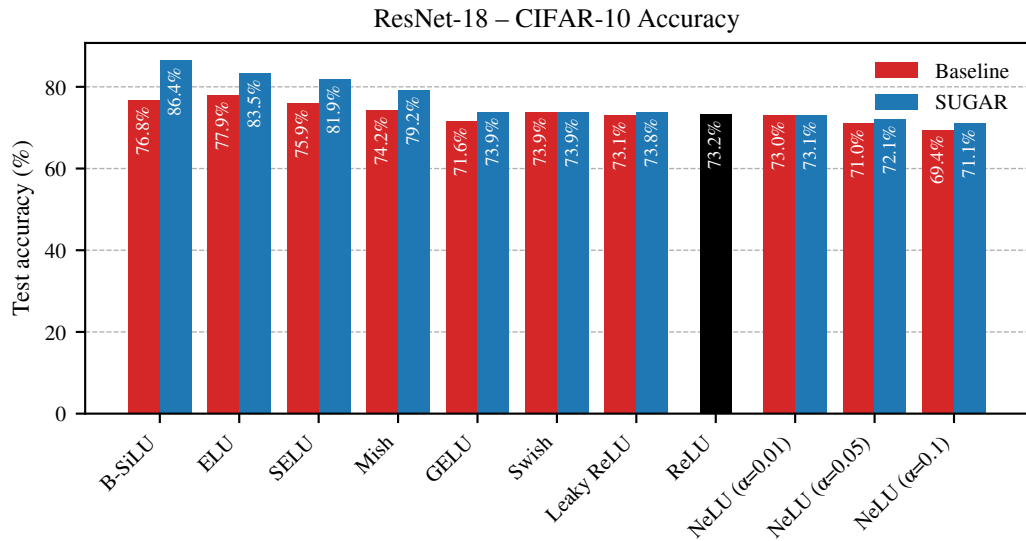


Figure 12: Test accuracy of ResNet-18 on CIFAR-10, comparing baseline to SUGAR.

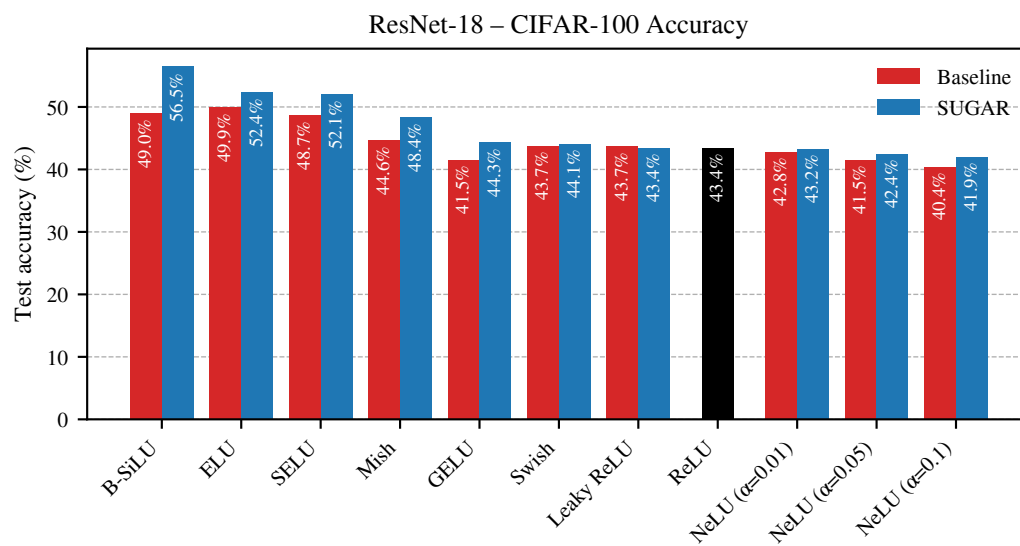


Figure 13: Test accuracy of ResNet-18 on CIFAR-100, comparing baseline to SUGAR.

F Experimental setup for Swin Transformer

The model is taken from the original work [23]. In this study, the tiny version of Swin Transformer (28M parameters) is used. Although our implementation is completely in line with [23], we provide detailed specifications regarding the training procedure here. Swin Transformer was trained on the Tiny ImageNet dataset with 200 classes.

- **Batch size:** We used a batch size of 200 for training.
- **Validation split:** 5% of the training set
- **Data augmentation:** Several augmentation techniques are employed during training:
 - Color jitter with intensity 0.4
 - AutoAugment policy: `rand-m9-mstd0.5-inc1`
 - Random erasing with:
 - * Probability: 0.25
 - * Mode: `pixel`
 - * Count: 1
 - Mixup with alpha 0.8
 - Cutmix with alpha 1.0
 - Mixup and Cutmix applied in batch mode with a switch probability of 0.5
- **Number of workers:** 8
- **Optimizer:** AdamW optimizer is used with the following parameters:
 - Betas: (0.9, 0.999)
 - Epsilon: $1e-8$
 - Weight decay: 0.05
- **LR schedule:** A cosine learning rate scheduler was used, with:
 - Base learning rate: $5e-4$, scaled linearly with batch size and number of devices
 - Warmup learning rate: $5e-7$
 - Minimum learning rate: $5e-6$
 - Warmup epochs: 20
 - Gradient clipping with max norm: 5.0
- **Epochs:** The model was trained for 300 epochs.
- **Repetitions:** 5 independent runs per configuration with seeds [1, 10, 20, 25, 42]
- **Hardware:** NVIDIA GeForce RTX 4090 25GB GPU (CUDA 12.4, Driver 550.144.03)

G Experimental setup for Conv2NeXt

The model is taken from the original work [5]. Following the settings in [5], the base version of Conv2NeXt (7M parameters) is used. Although our implementation is completely in line with [5], we provide detailed specifications regarding the training procedure here. `torch.compile` is applied with SUGAR. Conv2NeXt was trained on the CIFAR-100 dataset.

- **Batch size:** A per-GPU batch size of 200 was used, with gradient accumulation over 4 step, yielding an effective batch size of 800.
- **Validation/training set:** 50000 / 10000 as in default CIFAR-100 setting in torchvision. In accordance with [5], no test set was used.
- **Data augmentation:** Following augmentation strategies were deployed:
 - AutoAugment: `rand-m9-mstd0.5-inc1`
 - Color jitter: 0.4
 - Random erasing with:
 - * Probability: 0.25
 - * Mode: `pixel`
 - * Count: 1
 - Mixup: `alpha=0.8`
 - Cutmix: `alpha=1.0`
 - Combined Mixup/Cutmix applied in batch mode with switch probability 0.5
- **Number of workers:** 10
- **Optimizer:** AdamW optimizer is used with the following parameters:
 - Learning rate: `4e-3`
 - Weight decay: 0.05
 - Epsilon: `1e-8`
 - Betas: default `((0.9, 0.999))`
- **LR schedule:** A cosine learning rate scheduler was used:
 - Initial learning rate: `4e-3`
 - Minimum learning rate: `1e-6`
 - Warmup period: 20 epochs
 - Weight decay followed a cosine schedule as well
- **Epochs:** Training was performed over 300 epochs.
- **Repetitions:** 5 independent runs per configuration with seeds [1, 10, 20, 25, 42]
- **Hardware:** NVIDIA H100 80GB GPU (CUDA 12.4, Driver 550.127.08)